Astronomical & Astrophysical Transactions

The Journal of the Eurasian Astronomical Society

The turbulence in free shear flows and in accretion discs

O. M. Belotserkovskii [a]; V. M. Chechetkin [b]; S. V. Fortova [a]; A. M. Oparin [b]; Yu. P. Popov [b]; A. Yu. Lugovsky [b]; S. I. Mukhin [c]
[a] Institute for Computer Aided Design, Russian Academy of Sciences, Moscow, Russia
[b] Institute of Applied Mathematics, Russian Academy of Sciences, Moscow, Russia
[c] Moscow State University, Moscow, Russia

PLEASE SCROLL DOWN FOR ARTICLE

Taylor & Francis
Taylor & Francis Group

The turbulence in free shear flows and in accretion discs

O. M. BELOTSERKOVSKII*†, V. M. CHECHETKIN‡, S. V. FORTOVA†,
A. M. OPARIN†, YU. P. POPOV‡, A. YU. LUGOVSKY‡ and S. I. MUKHIN§

†Institute for Computer Aided Design, Russian Academy of Sciences, Moscow, Russia
‡Institute of Applied Mathematics, Russian Academy of Sciences, Moscow, Russia
§Moscow State University, Moscow, Russia

Physical models of the development of turbulence in free shear flows and in accretion discs are proposed. The models are based on the results of numerical simulations of turbulent flow development. The main idea of the proposed theory of turbulence in free shear flow is stated as follows: the onset of turbulence begins with the formation of large vortices. The formation and evolution of large-scale turbulence in accretion discs are considered. It is shown that the kinetic energy of vortices forming in a turbulent flow is a virtually constant fraction of the initial kinetic energy of the rotating matter of an accretion disc. A possible mechanism explaining the transfer of angular momentum by large vortices that form in the disc without any noticeable heating of the matter is suggested.

Keywords: Accretion discs; Large-scale turbulence; Angular momentum transfer

1. Introduction

The problem of turbulence has challenged scientists for over a century. However, no comprehensive turbulence theory has been developed to this day.

In 1985, Belotserkovskii [1] showed that fully developed free turbulence could be simulated without using any subgrid-scale model and adjustment of any semiempirical constants. The most systematic presentations of this approach can be found in [2, 3], where it was applied to free turbulent flows behind moving bodies (including both near- and far-wake flow structures), oceanic flows, Taylor–Couette flow, evolution of turbulent mixing zones, and other important problems concerning the onset of turbulence. The approach reflects the multidimensional and unsteady nature of the flows in question and takes into account phenomena related to compressibility, as well as effects due to viscosity (dominated by molecular mechanism). In those studies, it was also shown that large-scale vortices play a dominant role in turbulent flow structure.

The basic ideas of direct numerical simulation of turbulence rely on the following two hypotheses supported by experimental evidence.

*Corresponding author. Email: a.oparin@icad.org.ru

(i) Large-scale coherent vortices and small-scale stochastic turbulence are statistically independent at high Reynolds numbers.
(ii) Molecular viscosity (more generally, the mechanism of energy dissipation) plays a minor role in the analysis of large-scale vortex dynamics.

Large vortices carry the greater part of the energy of turbulent motion and determine the flow structure, but they do not result in the dissipation of kinetic energy into heat. Such dissipation is connected with small-scale turbulence. The dynamics of large vortices do not reflect the structure of random fluctuations, being governed by the Navier–Stokes equations in which the inertial terms dominate over the viscous terms. Accordingly, the structure of a vortex develops as a result of the combined action of pressure gradients and transient forces arising from velocity fields. Therefore, the formation of both large-scale vortices and the ensuing flow structure must be described by the Euler equations.

Theoretical research on the accretion discs that form around gravitating compact objects has also been conducted over many years. Recently, the problem of angular momentum transfer in accretion discs has become prominent. Researchers' interest in the problem is fuelled by an observed link between the temperature of an accretion disc and the intensity of radiation from the compact object during mass accretion onto the object. For intense mass accretion onto a central object, there must be processes in the disc which transfer angular momentum to its outer boundaries. In [4], turbulent viscosity was suggested for such a mechanism. It shows that the accretion rate determines the heating of the accretion disc due to molecular viscosity.

There have also been attempts to suggest magnetic viscosity for this mechanism. In [5], it was shown that even the presence of a weak magnetic field renders a hydrodynamically stable accretion disc unstable and results in turbulent flows inside the disc. This phenomenon was first considered in [6], which showed that certain distributions of the magnetic field and angular velocity result in an instability, which was termed magnetorotational instability. The appearance of this instability causes a redistribution of angular momentum and its transfer to outer boundaries of the disc.

The general belief is that the shear-flow turbulence viscosity is local and dynamic in character and results in local emission of heat [7]. An important problem is to explain the low temperature of the disc, which is much lower than the temperature that would account for the observed intensity of radiation at the given accretion rate. There are numerous studies which explore the conversion of the kinetic energy of turbulent flows not only into heat but also into other kinds of energy. This gave rise to an advection-dominated accretion [7].

In this paper, we consider the problem of the formation and evolution of large-scale turbulence flow from initially small disturbances. The problem is of significant interest as regards various disc flows under astrophysical conditions [8–11]. The formation of large-scale turbulence makes it possible for angular momentum to be transferred by large turbulent structures that form in shear flow in the accretion disc. The transfer of angular momentum by large turbulent vortices does not result in any noticeable heating of matter. A process such as this provides the required accretion rate accompanied by a comparatively low temperature of the accretion disc. Thus, a new mechanism is suggested for the transfer of angular momentum in accretion discs, which yields accretion characterized by smaller local heat emission.

2. Two-dimensional modelling of free shear flows

To examine the physical scenarios of the onset of turbulence, we performed an extensive series of numerical simulations of free shear flows of an ideal compressible gas.

For simulations we used two-dimensional ($i = 1, 2$) Euler gas dynamics equations in Cartesian coordinates:

$$\frac{\partial \rho}{\partial t} + \nabla_i(\rho u_i) = 0,$$

$$\frac{\partial(\rho u_i)}{\partial t} + \nabla_j(\rho u_i u_j) = -\frac{\partial P}{\partial x_i} + \rho g_i,$$

$$\frac{\partial(\rho E)}{\partial t} + \nabla_j[(\rho E + P)u_j] = \rho g_i u_i,$$

$$\frac{\partial(\rho C)}{\partial t} + \nabla_i(\rho C u_i) = 0,$$

$$E = \varepsilon + \frac{u_i u_i}{2}.$$

The ideal gas law is used in the following form:

$$P = (\gamma - 1)\rho\varepsilon.$$

Here, t is the time, ρ is the gas density, p is the pressure, ε is the specific internal energy, E is the full specific energy, γ is the ratio of specific heats, u_i is the component of the gas velocity, g_i is the component of the gravitational acceleration and C is the virtual concentration for visualization.

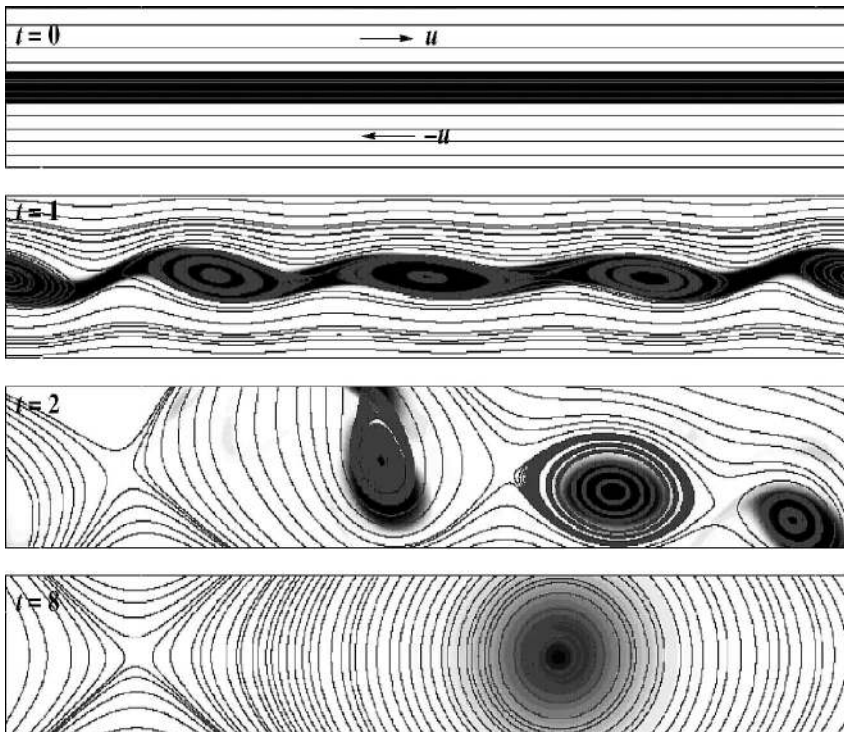We used monotonic dissipative stable finite-difference schemes with positive operators [1–3].

Figure 1. Development of large-scale vortices in a free turbulent shear layer. Streamlines are shown at instants separated by equal time intervals, including the starting moment. The grey-scale value represents the concentration of particles initially localized in the shear layer.
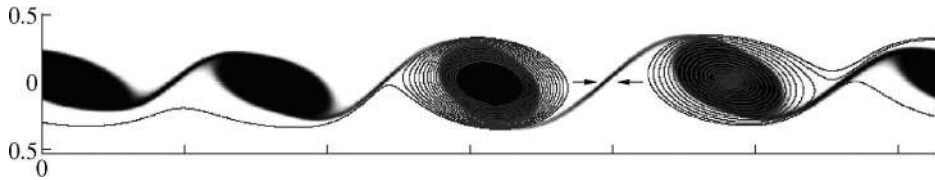
Figure 2. Attraction of vortices with similar vorticity signs.

We analysed the evolution of a shear layer with a uniform velocity gradient. Figure 1 demonstrates that large vortices of diameter comparable with the shear-layer thickness develop first. The vortex motion in a finite volume is generated by a pressure gradient. The shear layer breaks up into large vortices, and smaller eddies develop in their wakes. At the final instant of the simulation, the flow consists of a single vortex occupying the computational domain. This effect is explained by the attraction of vortices with similar vorticity signs due to the Zhoukovskij force (figure 2). The computation was performed with free-flow conditions set on the upper and lower boundaries combined with periodic conditions at the upstream and downstream boundaries.

Figure 3 shows the results obtained by computing the evolution of turbulence in a similar shear layer, but with impermeability conditions set on the upper and lower boundaries. Here, the onset of turbulence follows the scenario observed in the preceding simulation. However, the final turbulent flow has a complicated pattern involving both large-scale vortices and smaller structural elements. This result is due to interactions of the background flow with walls and large-scale vortices.

Figure 4 illustrates the evolution of a Taylor–Couette flow from an initial state in which the white fluid (with zero marker concentration) in the annular half-gap adjoining the inner cylinder is at rest and the black fluid (with unit marker concentration) in the outer half-gap rotates as a solid body having the angular velocity of the outer cylinder.
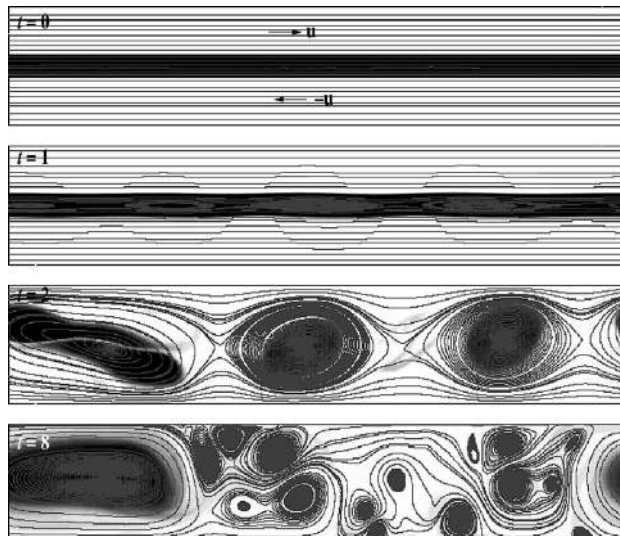

Figure 3. Flow analogous to that shown in figure 1, but confined between walls.
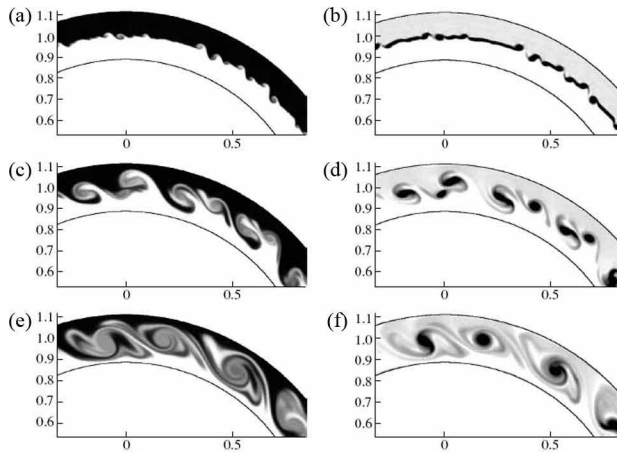
Figure 4. (a), (c), (e) 'Marker' concentrations and (b), (d), (f) vorticities in the Taylor–Couette flow at (a), (b) $t = 0.05$, (c), (d) $t = 0.1$ and (e), (f) $t = 0.2$. The outer cylinder is rotating counterclockwise; the inner cylinder is at rest.

The numerical results lead to the following conclusion about the onset of turbulence in a flow. The development of turbulence begins with the formation of large vortices. Well-developed turbulence should be modelled in the framework of the Euler equations, which correctly describe the distribution of basic length scales [1]. Multiple small eddies merge under the action of the Zhoukovskij force.

3. Three-dimensional modelling of free shear flows

To investigate the physical scenario of the onset of turbulence, we performed numerical simulations of free shear flows of an ideal compressible gas.

For simulations we used three-dimensional ($i = 1, 2, 3$) Euler gas dynamics equations in Cartesian coordinates with ideal gas law.

Let us consider the flow of matter in the integration domain ($0 \leqslant x \leqslant L_x$, $0 \leqslant y \leqslant L_y$, $-L_z/2 \leqslant z \leqslant L_z/2$). The initial velocity u_1 along the x direction is used in the following form:

$$u_1 = u_0, \qquad \frac{H}{2} \leqslant z \leqslant \frac{L_z}{2},$$

$$u_1 = -u_0, \qquad -\frac{L_z}{2} \leqslant z \leqslant -\frac{H}{2},$$

$$u_1 = \frac{u_0(2z)}{H}, \qquad -\frac{H}{2} \leqslant z \leqslant \frac{H}{2} \quad \text{(constant gradient of } u_1).$$

The initial velocity along the y direction is equal to zero. The initial velocity along the z direction has a small disturbance (1% of u_1) inside the shear layer.

The boundary conditions are the following: periodic conditions for the x and y directions, and impermeability conditions for the z direction.

Figure 5 shows the equiscalar surfaces of vorticity ($|\mathrm{rot}(u_1, u_2, u_3)|$) at successive time moments for calculation with $L_z = 1$, $H = 0.2$, $L_x = 2\pi$, $L_y = \pi$.

In this case the onset of shear instability begins with the formation of large-scale vortices. This time moment corresponds to $t = 3$ (figure 5). Further the instability is developed on the
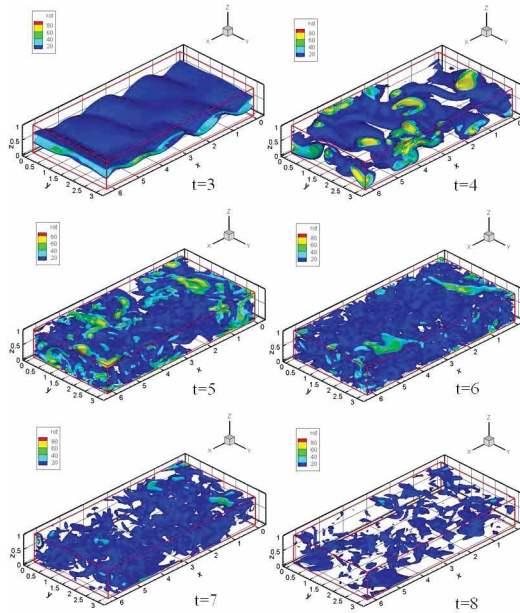
Figure 5. Equiscalar surfaces of the vorticity at successive time moments for a calculation with $L_z = 1$, $H = 0.2$, $L_x = 2\pi$ and $L_y = \pi$.

surface of large vortices. The formed structures interact with each other and the walls. The results of this process are shown in figure 5 at $t = 4$, $t = 5$, $t = 6$, $t = 7$ and $t = 8$.

Let us analyse the influence of the length of the shear layer on the evolution of the turbulence. Three variants with different shear layer lengths $L_y = 2\pi$, $\pi/2$ and $\pi/8$ and with $L_x = 2\pi$, $L_z = 2\pi$ and $H = 1$ were modelled. The results of these calculations are shown in figures 6–8. Note that the value of the specific concentration is equal to 1 inside the shear layer and to 0 outside for the initial time moment.

It is shown that the evolution of the flow at the beginning has a quasi-two-dimensional nature for all calculations (figures 6–8, $t = 8$). Further we can see that the nature of the evolution continues to be quasi-two-dimensional longer for lower values of L_y. For the last calculation (figures 6–8, $t = 20$) the flow possesses a quasi-two-dimensional nature to the end.

4. Large-scale turbulence in accretion discs

Using the hydrodynamic approach, we consider an accretion disc rotating around a central gravitating compact object (figure 9(a)). Assuming that the thickness of the accretion disc is very small compared with its radius, we shall solve the problem in two-dimensional geometry. Self-gravitation of the gas will be ignored.

Let the gas be an ideal compressible gas whose behaviour is described by a system of two-dimensional Euler gas dynamics equations with dimensionless variables in polar coordinates:

$$\frac{\partial(r\rho)}{\partial t} + \frac{\partial(r\rho u)}{\partial r} + \frac{1}{r}\frac{\partial(r\rho v)}{\partial \varphi} = 0,$$
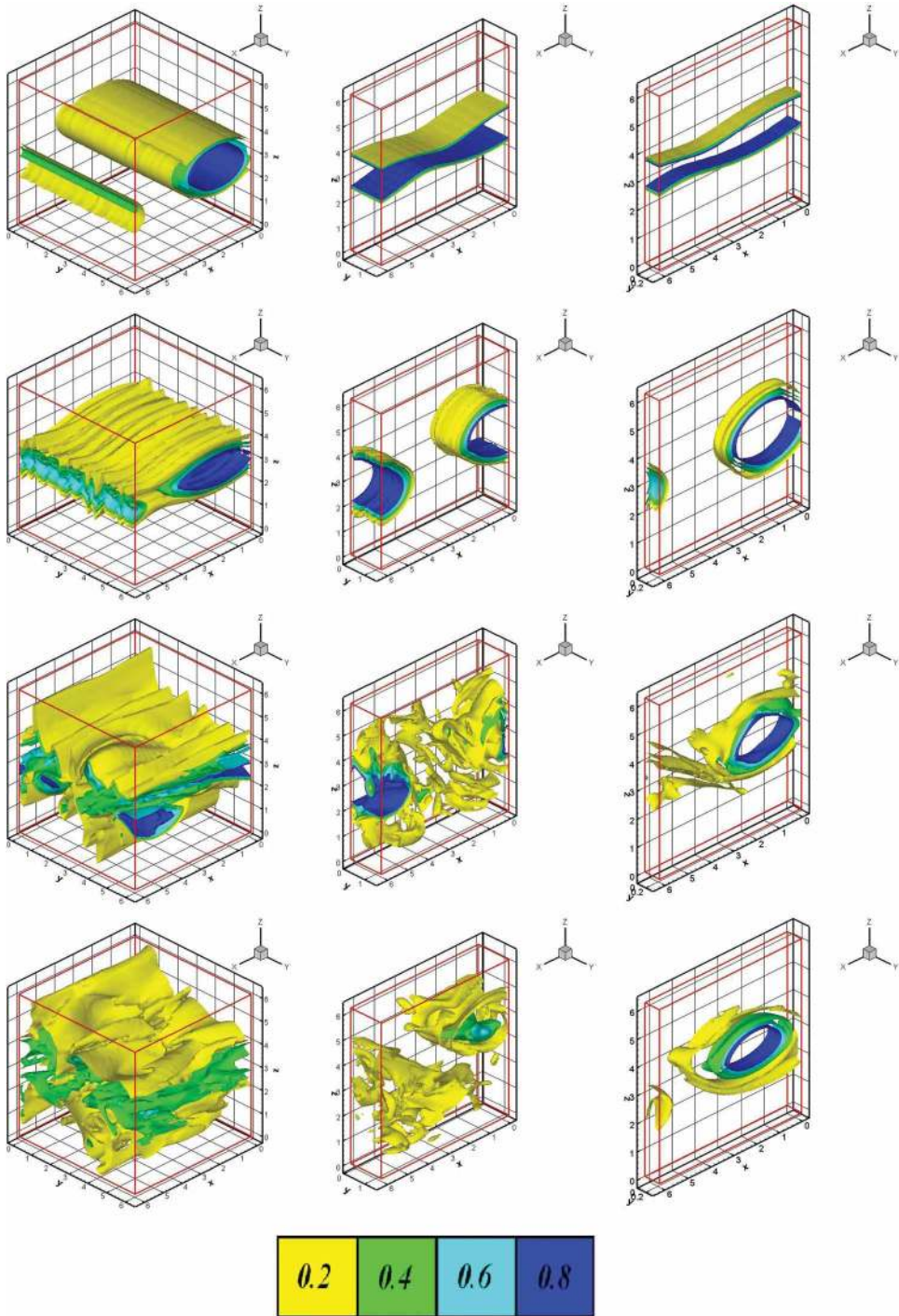
Figure 6. Equiscalar surfaces of the specific concentration. The time moments (from top to bottom) are $t = 8$, 12, 16 and 20. The lengths L_y of the shear layer are 2π, $\pi/2$ and $\pi/8$.
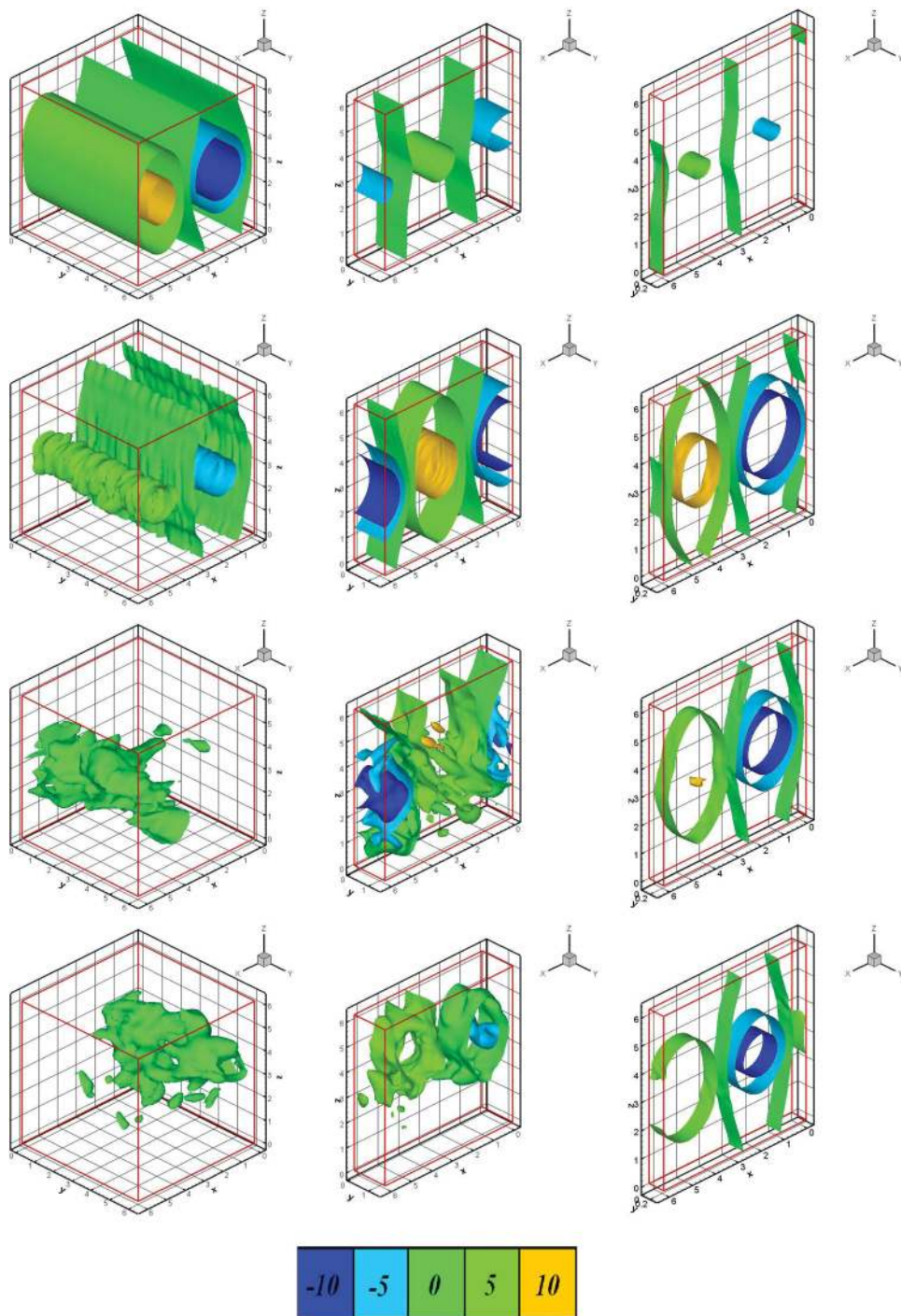
Figure 7. Equiscalar surfaces of the pressure. The time moments (from top to bottom) are $t = 8$, 12, 16 and 20. The lengths L_y of the shear layer are 2π, $\pi/2$ and $\pi/8$.
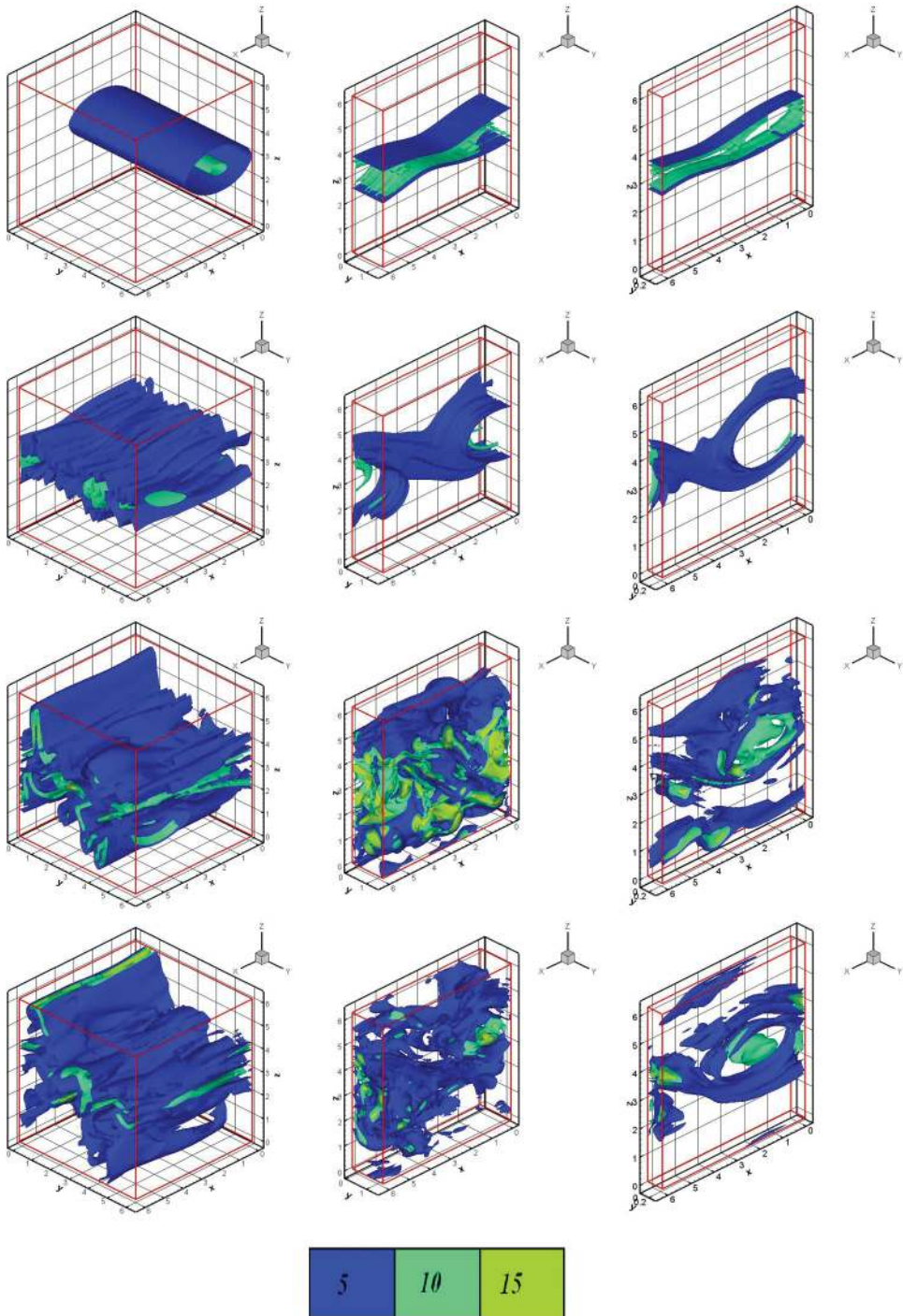
Figure 8. Equiscalar surfaces of the vorticity. The time moments (from top to bottom) are $t = 8$, 12, 16 and 20. The lengths L_y of the shear layer are 2π, $\pi/2$ and $\pi/8$.
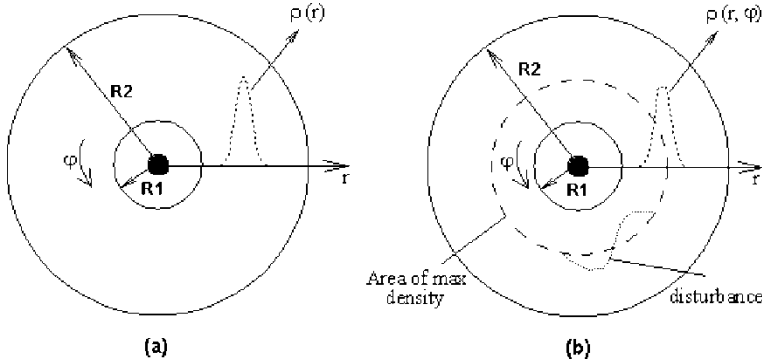
Figure 9.   Assumed area with (a) an equilibrium disc configuration and (b) a disc configuration with a disturbance.

$$\frac{\partial(r\rho u)}{\partial t} + \frac{\partial(r\rho u^2 + rp)}{\partial r} + \frac{1}{r}\frac{\partial(r\rho uv)}{\partial\varphi} = p + \rho v^2 + r\rho F_{\text{gr}},$$

$$\frac{\partial(r\rho v)}{\partial t} + \frac{\partial(r\rho vu)}{\partial r} + \frac{1}{r}\frac{\partial(r\rho v^2 + rp)}{\partial\varphi} = -\rho uv,$$

$$\frac{\partial(r\rho e)}{\partial t} + \frac{\partial(r\rho uh)}{\partial r} + \frac{1}{r}\frac{\partial(r\rho vh)}{\partial\varphi} = r\rho F_{\text{gr}}u,$$

$$e = \varepsilon + \frac{V^2}{2} = \varepsilon + \frac{u^2}{2} + \frac{v^2}{2}, \quad h = e + \frac{p}{\rho}.$$

The ideal gas law is used in the following form:

$$p = (\gamma - 1)\rho\varepsilon.$$

Here, r is the radius, φ is the azimuthal angle, t is the time, ρ is the gas density, p is the pressure, ε is the specific internal energy, e is the full specific energy, γ is the ratio of specific heats, h is the total enthalpy, $V = (u, v)$ is the gas velocity, u is its radial component, v is its azimuthal component and $F_{\text{gr}} = (-1/r^2)$ is the radial component of the specific gravitational force (here all variables are dimensionless).

Let us consider the flow of gas in the assumed area $\Omega = (R_1 \leqslant r \leqslant R_2) \times (0 \leqslant \varphi \leqslant 2\pi)$ (figure 9(a)). For the boundaries of the assumed region, we set free-flow boundary conditions. For the initial state of the accretion disc, we select the analytical solution $u_{\text{eq}} \equiv 0$, $v_{\text{eq}}(r) > 0$, $\rho_{\text{eq}}(r)$ and $p_{\text{eq}}(r)$ used in [12], which is an equilibrium state obtained in [13] for a two-dimensional model.

Note that the assumed region is selected so that its radius is about twice the typical radius of an accretion disc, *i.e.* the region where most of the mass of a disc is concentrated.

To approximate the differential equations, we use the total variation diminishing scheme [14–17].

To study the stability of accretion discs affected by small disturbances, let us introduce disturbances for the azimuthal velocity component in the maximum density area of a disc (figure 9(b)).

We use the grid $\omega = \omega_r \times \omega_\varphi$ as follows:

$$\omega_\varphi = \left\{ \varphi_j; \varphi_j = j \times h_\varphi; j = 0, \ldots, N_\varphi; h_\varphi = \frac{2\pi}{N_\varphi} \right\},$$

$$\omega_r = \left\{ r_i; r_i = R_1 + i \times h_r; i = 0, \ldots, N_r; h_r = \frac{R_2 - R_1}{N_r} \right\}.$$

The assumed area and the number N_r of points on r remain the same in all the variants of the task: $R_1 = 0.15$, $R_2 = 1.8$ and $N_r = 80$.

In all the calculations below, the width of the disturbance band with respect to r in the maximum density region is two grid cells. Here small sinusoidal disturbances for the azimuthal velocity component are inserted in the equilibrium state of the accretion disc given by

$$v(r, \varphi) = v_{\text{eq}}(r)[1 + A \sin(n\varphi)],$$

where $v_{\text{eq}}(r)$ is the azimuthal velocity in the stable state, A is the amplitude of the disturbances and n is the number of periods in the interval $0 \leqslant \varphi < 2\pi$.

Below we provide the results of two calculations with different initial disturbances of the velocity depending on the angle.

(i) *Variant 1.* First, we consider the case (which forms the basis for the subsequent investigation) where a disturbance with $A = 0.2$ and $n = 10$ is introduced for $0 \leqslant \varphi < 2\pi$. A grid ω is used, where $N_r = 80$ and $N_\varphi = 260$. Figure 10 shows the isolines of the density at different points in time and figure 11 shows isolines of the vorticity (rot$V$) at corresponding points in time. The last point is at the stage of the process which corresponds to a half-turn of the disc (the turn of the disc here represents the time required for the disc matter in the maximum density area to rotate fully around the gravitating object).

(ii) *Variant 2.* We now turn to another variant where disturbances are introduced at $A = 0.2$ and $n = 10$ in $(2\pi/10) \leqslant \varphi \leqslant (4\pi/10)$ and $(12\pi/10) \leqslant \varphi \leqslant (14\pi/10)$. The grid ω is
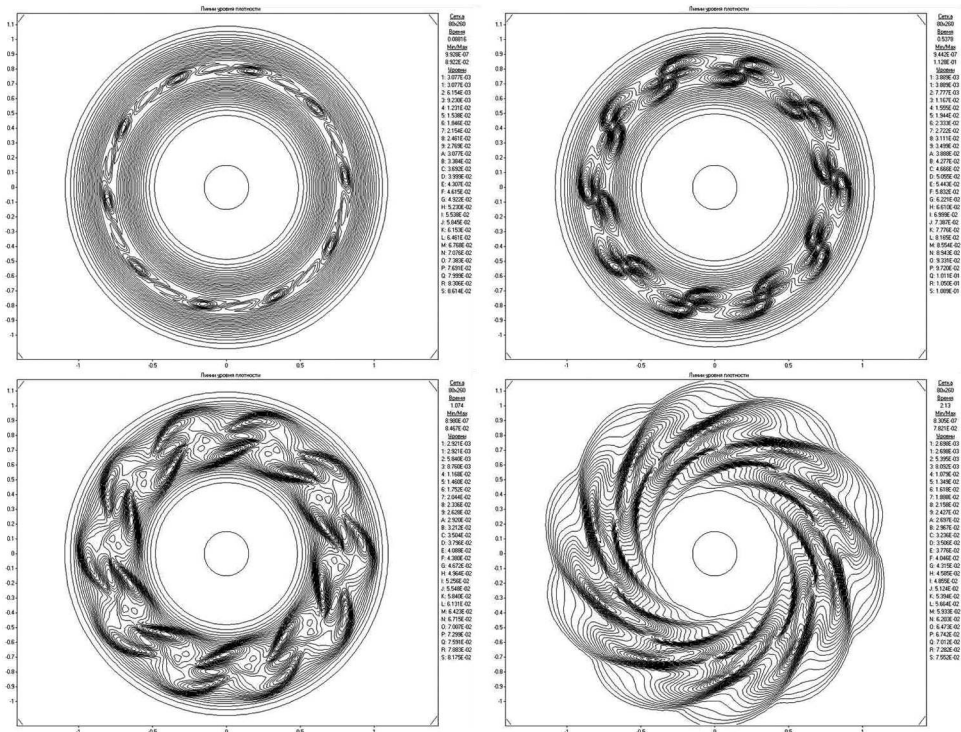

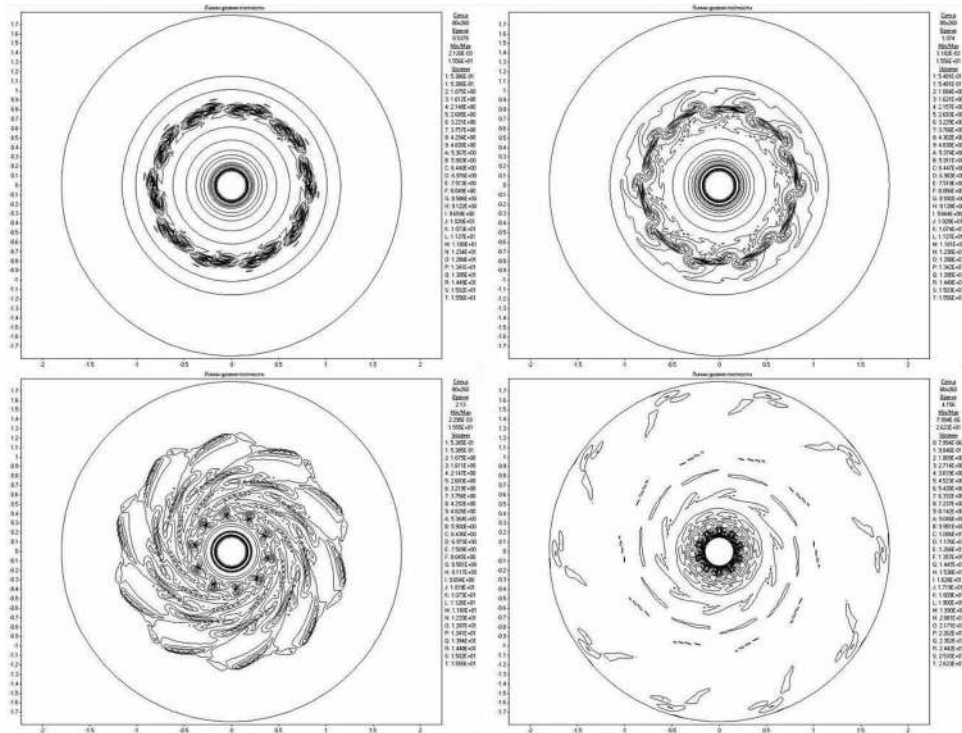Figure 10. Isolines of the density in variant 1.

Figure 11.   Isolines of the vorticity in variant 1.

used in the calculations, where $N_r = 80$ and $N_\varphi = 150$. Figures 12(a) and (b) show the vorticity isolines and density isolines respectively at an advanced stage of turbulence evolution which corresponds to two thirds of a turn of the disc.

These calculations show that small disturbances introduced into a stable disc evolve, resulting over time in large-scale turbulence structures which persist for a considerable period of time. This process cause a rearrangement of the flow in almost the entire region, although the disturbance was introduced into only a small part of the area. Note also that the two structures obtained in variant 2 are symmetrical and similar in quality to the structures from variant 1 (figures 10 and 11).
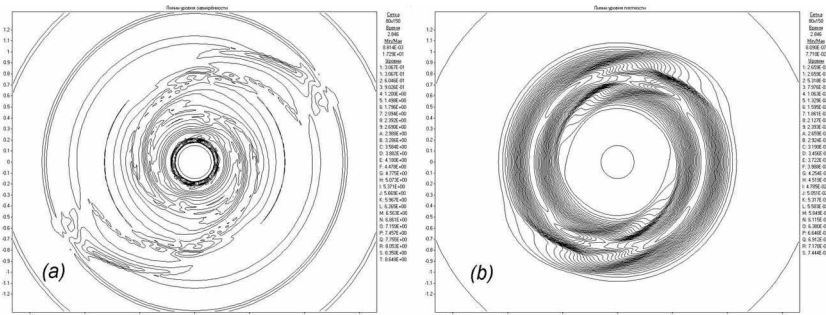

Figure 12.   (a) Vorticity isolines and (b) density isolines at two thirds of a turn in variant 2.
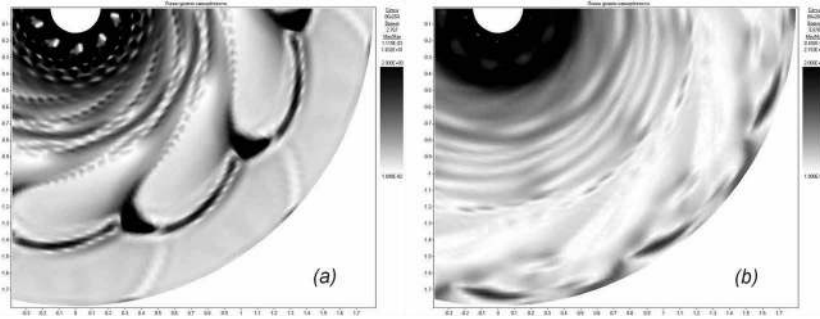
Figure 13. Vorticity at (a) two thirds of a turn and (b) 1.5 turns.

We made a series of calculations for amplitudes *A* ranging from 0.01 to 0.2, with disturbances introduced in one- or two-cell bands, with different numbers of local disturbances (ranging from 1 to 10 at $n = 10$ and from 1 to 20 at $n = 20$), and with various grids (from 40×130 to 320×1040). The results of the calculations show that the quality of the flow remains unchanged.

Taking the calculation (i) (figures 10 and 11) as an example, let us look more closely at the behaviour of the vorticity. Figures 13(a) and (b) show the character of vorticity in a part of the region at the times which correspond to two thirds of a turn and to 1.5 turns respectively. Large structures can be seen to form (figure 13(a)) which drift towards the outer boundary of the region (figure 13(b)). However, the low density of the matter at the outer boundary (which is lower than the density in the maximum-density region by the order of 5) means that there is almost no outflow of matter. Also, in figure 13(a), vortex trails can be observed, and structures are formed near the inner boundary of the area. It should be noted that it is very difficult to discern any structures in the internal and external parts of the assumed area on the density patterns because of the low density.

Consider also the character of the specific vorticity (($\mathrm{rot}V$)$/\rho$) in a part of the region (figure 14) at the times corresponding to a third of a turn (figure 14(a)) and a full turn (figure 14(b)). Figure 14(a) shows an instability that is starting to evolve and the formation of vortex trails. In figure 14(b), spiral structures are being formed (figures 10 and 11) and well-developed vortex trails are shown.

It is of some interest to observe the change in the kinetic energy of the turbulence. As mentioned above, first a disturbance of the azimuthal velocity component is introduced with amplitude *A* ranging from 0.01 to 0.2. This corresponds to a disturbance energy from 0.001%
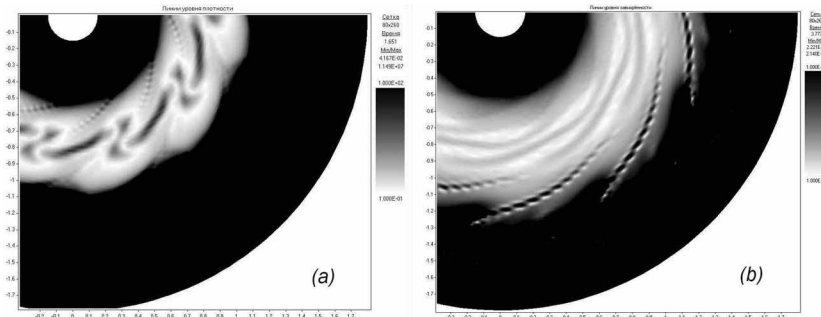

Figure 14. Specific vorticity at (a) one third of a turn and (b) one turn.
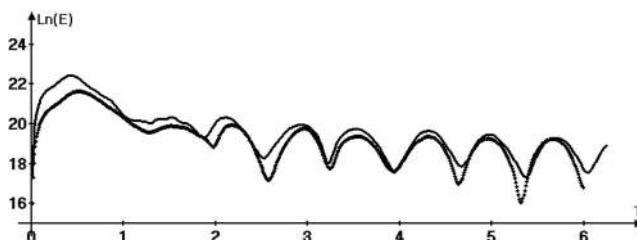
Figure 15.   Change in the kinetic energy of a turbulence over time (in disc turns) at initial disturbances of velocity with $A = 0.2$ (solid curve) and $A = 0.1$ (full diamonds).

to 0.3% of the total initial kinetic energy. Figure 15 shows the change in the kinetic energy of a turbulent flow over time (the kinetic energy of a turbulence here and below is the kinetic energy of the radial motion of gas in an accretion disc). Time is measured in turns of the disc; the initial disturbances of the velocity have amplitudes $A = 0.2$ and $A = 0.1$. On comparison of the two graphs, it can be seen that the maximum values are very different. Later, when reaching the quasistationary regime, the energy values are almost the same (by the quasistationary regime we mean the state where the kinetic energy of the turbulent flow changes little over time, oscillating around an almost constant value). For the variants with $A = 0.01$ and $A = 0.05$, the values of the quasistationary regime are approximately the same as the obtained results. Therefore, we can assume that, in the quasistationary regime, the kinetic energy of the turbulence is determined by the initial kinetic energy and is independent of the energy of the initial disturbance. This testifies to the physical validity of the assumption that large-scale turbulences evolve in shear flows in accretion discs and also confirms the fact that, once the disturbance formation has reached its peak, vortex structures do not disappear, the flow remains turbulent in character, and, as shown in figure 13(b), large structures transfer angular momentum to the outer boundaries of the disc.

Let us now analyse the change and redistribution of the angular momentum in the flow obtained in the principal calculation (figures 10 and 11).

Figure 16 shows the distribution of the angular momentum along the radius at the initial instant of time and at two full turns. Throughout the entire calculation, angular momentum is thrown out of the zone where most of the matter is concentrated on both sides of the radius and is redistributed. The maximum of the angular momentum decreases compared with the initial value, and the region where the angular momentum is mainly concentrated widens. At the graph which corresponds to two turns, the gas in front of the inner boundary of this region at time zero, and particularly behind the outer boundary, acquires considerable angular
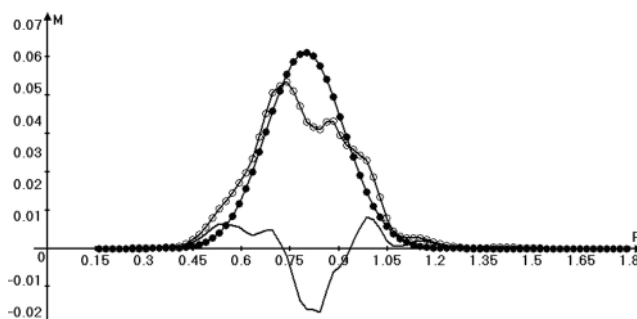

Figure 16.   Redistribution of the angular momentum along the radius ($\varphi = 0$) at times $t_1 = 0$ (full circles) and $t_2 = 2$ turns (open circles) and the difference between the angular momenta, $M(t_2) - M(t_1)$ (solid curve).
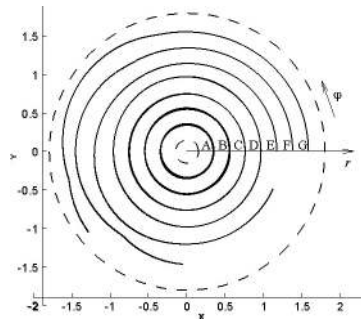
Figure 17. Trajectories for the gas particles.

momentum. The above-described redistribution of angular momentum can also be observed in the graph for the difference of the angular momenta at the time when the disc material has made two full turns and at time zero.

The overall angular momentum of the system remains almost unchanged, but it is redistributed along the radius. We should note that the mass of the gas in the system also remains virtually constant, i.e. the angular momentum is not redistributed owing to the flow of matter outside the boundaries.

Let us now consider the behaviour of the entropy $S = S_0 \ln(p/\rho^\gamma) + C$ ($S_0 = $ constant and $C = $ constant), and in particular how it changes over time. To achieve this, we set seven equidistant points on the axis $\varphi = 0$ at time $t = 0$ and build seven trajectories for gas particles that were at these points at time zero (figure 17). If we know the field of velocity at each check point, we can draw a trajectory for the gas particles with very good accuracy. The deviation from the mean value of entropy is about 5% along the entire trajectory which lies in the region of maximum density and angular momentum (figure 18(a)) (this is the region where initial disturbances are introduced and vortices are formed). Taking into account the approximate calculation of the particle trajectory in Euler coordinates and the error margin that is inevitable in this case, we can assume that the entropy S along this trajectory is a constant value. For other trajectories, the deviation from the mean value does not exceed 1.5% (figure 18(b)), which is also evidence of constant entropy along the trajectories. Therefore, the entropy in the system is constant.
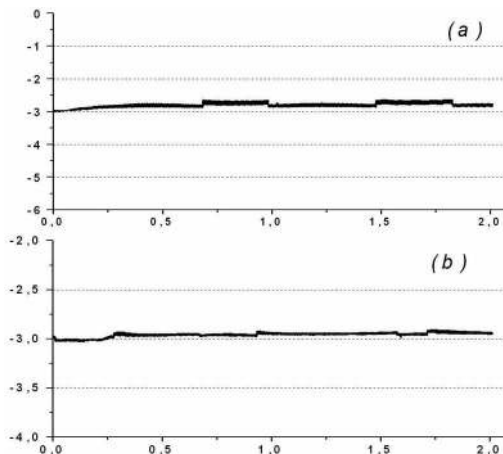

Figure 18. Entropy along (a) trajectory C and (b) trajectory D in figure 17. The time is in turns around the disc.

Remember that there is no viscosity and heat conduction in the system, and the scheme viscosity is small. The constant entropy means that the flow is almost adiabatic. Consequently, the turbulent viscosity is low and cannot act as a mechanism for the redistribution of the angular momentum. Thus, the redistribution of the angular momentum observed in the calculations is related to the formation of large structures. It is these very structures that transfer the angular momentum.

5. Conclusions

In free shear flow the origin of turbulence is connected with large scales. The Zhoukovskij force plays an important role in the evolution of turbulence. The ratio L_y/L_x determines the two-dimensional assumption. If $(L_y/L_x) \ll 1$, then the two-dimensional model can be used. The thin accretion disc concerned in our calculation satisfies this condition.

The disc configuration studied in this paper, with density at the boundaries that is several orders smaller than the density in the centre, was chosen so as to exclude any impact of boundary conditions.

The calculations carried out enable us to make several conclusions as to the development of small disturbances. Small disturbances, introduced in a relatively small region of an accretion disc in the state of stability, develop into large structures and spread over a considerable portion of the assumed region. The resulting flow is turbulent in character.

These large structures play a major role in the redistribution of the total angular momentum in accretion discs without any noticeable heating of the disc material. However, there is no evidence in the calculations of any reductions in the total angular momentum of the disc material, nor of any ejection of material.

Acknowledgements

References

[1] O.M. Belotserkovskii, Zh. Vychisl. Mat. Mat. Fiz. **25** 1856 (1985).
[2] O.M. Belotserkovskii, *Turbulence and Instabilities* (Edwin Mellen, Lewiston, New York, 2000).
[3] O.M. Belotserkovskii, A.M. Oparin and V.M. Chechetkin, *Turbulence: New Approaches* (Nauka, Moscow, 2002).
[4] N.I. Shakura, Soviet Astron. **16** 756 (1973).
[5] S. Balbus and J. Hawley, Astrophys. J. **376** 214 (1991).
[6] Ye.P. Velikhov, Zh. Exp. Teor. Fiz. **36** 1399 (1959).
[7] R. Narayan and I. Yi, Astrophys. J. **452** 710 (1995).
[8] J.G. Lominadze, G.D. Chagelishvili and R.G. Chanishvili, Soviet Astron. Lett. **14** 364 (1988).
[9] G.D. Chagelishvili, J.P. Zahn, A.G. Tevzadze *et al.*, Astron. Astrophys. **402** 401 (1988).
[10] A.G. Tevzadze, G.D. Chagelishvili, J.P. Zahn *et al.*, Astron. Astrophys. **408** 779 (2003).
[11] G. Bodo, G.D. Chagelishvili, G. Murante *et al.*, Astron. Astrophys. **437** 9 (2005).
[12] M.V. Abakumov, S.I. Mukhin, Yu.P. Popov *et al.*, Astron. Rep. **47** 11 (2003).
[13] M.V. Abakumov, S.I. Mukhin, Yu.P. Popov *et al.*, Astron. Rep. **40** 366 (1996).
[14] P.L. Roe, A. Rev. Fluid Mech. **18** 337 (1986).
[15] S. Osher and F. Solomon, Math. Comput. **38** 339 (1982).
[16] S. Chakravarthy and S. Osher, AIAA paper 85-0363 (1985).
[17] B. Einfeld, SIAM J. Numer. Anal. **25** 294 (1988).